PERGAMON

International Journal of Solids and Structures 40 (2003) 3311–3330

INTERNATIONAL JOURNAL OF SOLIDS and STRUCTURES

www.elsevier.com/locate/ijsolstr

Nonlinear bending and post-buckling of a functionally graded circular plate under mechanical and thermal loadings

L.S. Ma, T.J. Wang *

Department of Engineering Mechanics, Xi'an Jiaotong University, Xi'an 710049, China

Received 21 August 2002; received in revised form 31 January 2003

Abstract

Based on the classical nonlinear von Karman plate theory, axisymmetric large deflection bending of a functionally graded circular plate is investigated under mechanical, thermal and combined thermal–mechanical loadings, respectively, and axisymmetric thermal post-buckling behavior of a functionally graded circular plate is also investigated. The mechanical and thermal properties of functionally graded material (FGM) are assumed to vary continuously through the thickness of the plate, and obey a simple power law of the volume fraction of the constituents. Governing equations for the problem are derived, and then a shooting method is employed to numerically solve the equations. Effects of material constant n and boundary conditions on the temperature distribution, nonlinear bending, critical buckling temperature and thermal post-buckling behavior of the FGM plate are discussed in details.

Keywords: FGM; Nonlinear bending; Buckling; Post-buckling; Thermal and mechanical loading; Circular plate; Shooting method

1. Introduction

Extensive investigations on the thermal bending and post-buckling of isotropic and composite plates and shells were carried out by Tauchert and Huang (1987); Tauchert (1991); Meyers and Hyer (1991) and Leissa (1992), etc. However, there are few works on the stability, vibration, bending and buckling behavior of functionally graded structures, and these are still open problems. Loy et al. (1999) and Pradhan et al. (2000) examined the free vibration of functionally graded cylindrical shell by using the Rayleigh–Ritz method. An analytical solution of the dynamic response of simply supported functionally graded cylinder due to low-velocity impact was given by Gong et al. (1999). Based on the classical small deflection theory of plate, Yang and Shen (2001) investigated the dynamic response of a functionally graded rectangular thin plate with initial stress subjected to partially distributed impulsive lateral loads and without or resting on an

* Corresponding author. Tel.: +86-29-2668757; fax: +86-29-3237910.
E-mail address: wangtj@mail.xjtu.edu.cn (T.J. Wang).

0020-7683/03/$ - see front matter © 2003 Elsevier Science Ltd. All rights reserved.
doi:10.1016/S0020-7683(03)00118-5

foundation. Ng et al. (2000, 2001) studied the dynamic stability of functionally graded rectangular plate and cylindrical shell, respectively. A modified classical lamination theory to account for piezoelectric coupling terms under applied electric field was developed by Almajid et al. (2001), and then the theory was applied to predict the out-of-plane displacement and stress field of actuators and the functionally graded material (FGM) bimorph. Mian and Spencer (1998) established a large class of exact solutions of the three-dimensional elasticity equations for functionally graded and laminated elastic materials.

The response of functionally graded ceramic–metal plate accounting for the transverse shear strains, rotary inertia and moderately large rotations in the von Karman sense was studied by Praveen and Reddy (1998), in which finite element method was employed to investigate the static and dynamic responses of the functionally graded plate by varying the volume fraction of the ceramic and metallic constituents. Effect of imposed temperature field on the response of the functionally graded plate was also discussed. Reddy and Chin (1998) investigated the dynamic thermo-elastic response of functionally graded cylinders and plates. A thermo-elastic boundary value problem was derived by using the first-order shear deformation plate theory that account for coupling with a three-dimensional heat conduction equation for a functionally graded plate. Using the first-order shear deformation theory of Mindlin plate, axisymmetric bending of functionally graded annular and circular plates was studied by Reddy et al. (1999), in which the solutions were expressed in terms of the classical solutions based on the Kirchhoff plate theory. Based on the higher-order shear deformation theory of plate, Reddy (2000) developed both theoretical and finite element formulations for thick FGM plates, and the nonlinear dynamic responses of FGM plates subjected to suddenly applied uniform pressure were studied. Based on the von Karman theory, Woo and Meguid (2001) derived an analytical solution expressed in terms of Fourier series for the large deflection of functionally graded plates and shallow shells under transverse mechanical loading and a temperature field. Cheng and Batra (2000) studied three-dimensional thermo-mechanical deformations of an isotropic linear thermo-elastic functionally graded elliptic plate. A closed form solution was obtained which shows that the through-thickness distribution of the in-plane displacements and transverse shear stress in a functionally graded plate do not agree with those assumed in classical and shear deformation plate theories. Moreover, a new set of field equations in terms of displacement and stress potential functions for inhomogeneous plates had been presented and reformulated by Cheng (2001), and mixed Fourier series technique was employed to solve the equations. Using an asymptotic method, the three-dimensional thermo-mechanical deformations of functionally graded rectangular plate were investigated by Reddy and Cheng (2001) and the distributions of temperature, displacements and stresses in the plate were calculated for different volume fraction of ceramic constituent.

Assuming that the material properties throughout the structure are produced by a spatial distribution of the local reinforcement volume fraction $v_f = v_f(x, y, z)$, Feldman and Aboudi (1997) studied the elastic bifurcation buckling of functionally graded plate under in-plane compressive loading. More recently, Javaheri and Eslami (2002a,b) studied the thermal buckling of functionally graded rectangular plate based on the classical and the higher-order shear deformation theories of plate, respectively, and obtained the closed form solutions under several types of thermal loads. Ma and Wang (in press) studied the axisymmetric post-buckling behavior of a functionally graded circular plate under uniformly distributed radial compression on the basis of classical nonlinear plate theory.

To the authors' knowledge, only few works on the nonlinear bending of functionally graded plates are concerned, but the thermal post-buckling of FGM plates has not been carried out in the previous works. In the present paper, axisymmetric nonlinear bending and thermal post-buckling behavior of a functionally graded circular plate are studied under mechanical, thermal and combining thermal–mechanical loading in the framework of von Karman plate theory. Simply supported and clamped boundary conditions are considered. The material properties are assumed to vary continuously through the thickness of the plate. Effects of material properties and boundary conditions on the large deflection bending and thermal post-buckling behavior of the FGM plate are discussed in details.

2. Basic equations

A functionally graded circular plate with thickness h and radius b is considered here. It is assumed that the mechanical and thermal properties of FGM vary through the thickness of plate, and the material properties P can be expressed as (Reddy and Chin, 1998; Reddy et al., 1999)

$$P(z) = (P_{\mathrm{m}} - P_{\mathrm{c}})V_{\mathrm{m}} + P_{\mathrm{c}}, \tag{1}$$

where the subscripts m and c denote the metallic and ceramic constituents, respectively, V_{m} denotes the volume fraction of metal and follows a simple power law as

$$V_{\mathrm{m}} = \left(\frac{h - 2z}{2h}\right)^{n}, \tag{2}$$

where z is the thickness coordinate ($-h/2 \leqslant z \leqslant h/2$), and n is a material constant. According to this distribution, bottom surface ($z = -h/2$) of the functionally graded plate is pure metal, the top surface ($z = h/2$) is pure ceramics, and for different values of n one can obtain different volume fractions of metal.

Based on the classical nonlinear von Karman plate theory, the equilibrium equations of a thin plate subjected to a thermal load T and uniformly distributed transverse mechanical load q are as follows

$$(rN_r)_{,r} - N_\theta = 0, \tag{3}$$

$$(rQ_r)_{,r} + (rN_rW_{,r})_{,r} = -rq, \tag{4}$$

$$(rM_r)_{,r} - M_\theta - rQ_r = 0, \tag{5}$$

where the comma followed by r denotes differentiation with respect to r, W is the displacement in z direction, and the force and moment components N and M are as follows,

$$(N_r, N_\theta) = \int_{-h/2}^{h/2} (\sigma_r, \sigma_\theta)\mathrm{d}z, \tag{6a}$$

$$(M_r, M_\theta) = \int_{-h/2}^{h/2} (\sigma_r, \sigma_\theta)z\,\mathrm{d}z. \tag{6b}$$

The constitutive relations for the FGMs are given by

$$\begin{Bmatrix} \sigma_r \\ \sigma_\theta \end{Bmatrix} = \frac{E(z)}{1 - v^2}\begin{Bmatrix} 1 & v \\ v & 1 \end{Bmatrix}\left(\begin{Bmatrix} \varepsilon_r^0 \\ \varepsilon_\theta^0 \end{Bmatrix} + z\begin{Bmatrix} \kappa_r \\ \kappa_\theta \end{Bmatrix}\right) - \frac{E(z)}{1 - v}\alpha(z)T(z)\begin{Bmatrix} 1 \\ 1 \end{Bmatrix}. \tag{7}$$

The Young's modulus $E(z)$ and thermal expansion coefficient $\alpha(z)$ in Eqs. (7) follow the distribution law of Eqs. (1) and (2), namely,

$$E(z) = (E_{\mathrm{m}} - E_{\mathrm{c}})V_{\mathrm{m}} + E_{\mathrm{c}},$$

$$\alpha(z) = (\alpha_{\mathrm{m}} - \alpha_{\mathrm{c}})V_{\mathrm{m}} + \alpha_{\mathrm{c}}.$$

For simplicity, the Poisson's ratio v in Eqs. (7) is assumed to be a constant. The radial and circumferential strain components ε_r^0 and ε_θ^0 in the mid-plane of the plate (i.e. $z = 0$) can be calculated as

$$\varepsilon_r^0 = \frac{\mathrm{d}U}{\mathrm{d}r} + \frac{1}{2}\left(\frac{\mathrm{d}W}{\mathrm{d}r}\right)^2, \tag{8a}$$

$$\varepsilon_\theta^0 = \frac{U}{r} \tag{8b}$$

with U being the displacement in r direction. Variations of the curvature κ_r and κ_θ in the mid-plane of the plate ($z = 0$) can be calculated as,

$$\kappa_r = -\frac{\mathrm{d}^2 W}{\mathrm{d}r^2}, \tag{9a}$$

$$\kappa_\theta = -\frac{1}{r}\frac{\mathrm{d}W}{\mathrm{d}r}. \tag{9b}$$

The temperature difference $T(z)$ from the stress free state is governed by the following well-known heat transfer equation

$$-\frac{\mathrm{d}}{\mathrm{d}z}\left(K(z)\frac{\mathrm{d}T(z)}{\mathrm{d}z}\right) = 0 \tag{10}$$

with the boundary conditions $T(h/2) = T_1$ and $T(-h/2) = T_2$. The thermal conductivity coefficient $K(z)$ in Eq. (10) follows the distribution law of Eqs. (1) and (2), namely,

$$K(z) = (K_\mathrm{m} - K_\mathrm{c})V_\mathrm{m} + K_\mathrm{c}.$$

It is easily to obtain from Eq. (10) that

$$T(z) = T_2 + (T_1 - T_2)\int_{-h/2}^{z}\frac{\mathrm{d}z}{K(z)}\Big/\int_{-h/2}^{h/2}\frac{\mathrm{d}z}{K(z)}. \tag{11}$$

From Eqs. (6) and (7), one obtains

$$\begin{pmatrix} N_r \\ N_\theta \end{pmatrix} = \begin{bmatrix} A_{11} & A_{12} \\ A_{12} & A_{22} \end{bmatrix}\begin{pmatrix} \varepsilon_r^0 \\ \varepsilon_\theta^0 \end{pmatrix} + \begin{bmatrix} B_{11} & B_{12} \\ B_{12} & B_{22} \end{bmatrix}\begin{pmatrix} \kappa_r \\ \kappa_\theta \end{pmatrix} - \begin{pmatrix} N_r^\mathrm{T} \\ N_\theta^\mathrm{T} \end{pmatrix}, \tag{12}$$

$$\begin{pmatrix} M_r \\ M_\theta \end{pmatrix} = \begin{bmatrix} B_{11} & B_{12} \\ B_{12} & B_{22} \end{bmatrix}\begin{pmatrix} \varepsilon_r^0 \\ \varepsilon_\theta^0 \end{pmatrix} + \begin{bmatrix} D_{11} & D_{12} \\ D_{12} & D_{22} \end{bmatrix}\begin{pmatrix} \kappa_r \\ \kappa_\theta \end{pmatrix} - \begin{pmatrix} M_r^\mathrm{T} \\ M_\theta^\mathrm{T} \end{pmatrix}, \tag{13}$$

where A_{ij}, B_{ij} and D_{ij} are stiffness coefficients of the plate and can be calculated as

$$(A_{ij}, B_{ij}, D_{ij}) = \int_{-h/2}^{h/2} Q_{ij}(1, z, z^2)\,\mathrm{d}z \tag{14}$$

with

$$Q_{11} = Q_{22} = \frac{E(z)}{1 - v^2}, \quad Q_{12} = vQ_{11}.$$

The forces and moments in Eqs. (12) and (13) induced by thermal load can be calculated as

$$N_r^\mathrm{T} = \int_{-h/2}^{h/2}\frac{E(z)}{1 - v}\alpha(z)T(z)\,\mathrm{d}z, \tag{15a}$$

$$N_\theta^\mathrm{T} = \int_{-h/2}^{h/2}\frac{E(z)}{1 - v}\alpha(z)T(z)\,\mathrm{d}z, \tag{15b}$$

$$M_r^\mathrm{T} = \int_{-h/2}^{h/2}\frac{E(z)}{1 - v}\alpha(z)T(z)z\,\mathrm{d}z, \tag{15c}$$

$$M_\theta^{\mathrm{T}} = \int_{-h/2}^{h/2} \frac{E(z)}{1-v}\alpha(z)T(z)z\,\mathrm{d}z. \tag{15d}$$

From Eqs. (3)–(5), (8), (9), (12), (13) and (15), one then obtains the governing equations expressed in terms of the displacements

$$A_{11}\left[\frac{\mathrm{d}^2U}{\mathrm{d}r^2}+\frac{1}{r}\frac{\mathrm{d}U}{\mathrm{d}r}-\frac{U}{r^2}+\frac{\mathrm{d}^2W}{\mathrm{d}r^2}\frac{\mathrm{d}W}{\mathrm{d}r}+\frac{1-v}{2r}\left(\frac{\mathrm{d}W}{\mathrm{d}r}\right)^2\right] = B_{11}\left(\frac{\mathrm{d}^3W}{\mathrm{d}r^3}+\frac{1}{r}\frac{\mathrm{d}^2W}{\mathrm{d}r^2}-\frac{1}{r^2}\frac{\mathrm{d}W}{\mathrm{d}r}\right), \tag{16}$$

$$\begin{aligned} &D_{11}\left(\frac{\mathrm{d}^4W}{\mathrm{d}r^4}+\frac{2}{r}\frac{\mathrm{d}^3W}{\mathrm{d}r^3}-\frac{1}{r^2}\frac{\mathrm{d}^2W}{\mathrm{d}r^2}+\frac{1}{r^3}\frac{\mathrm{d}W}{\mathrm{d}r}\right)\\ &\quad= A_{11}\left[\frac{\mathrm{d}U}{\mathrm{d}r}+\frac{v}{r}U+\frac{1}{2}\left(\frac{\mathrm{d}W}{\mathrm{d}r}\right)^2\right]\frac{\mathrm{d}^2W}{\mathrm{d}r^2}+A_{11}\left[v\frac{\mathrm{d}U}{\mathrm{d}r}+\frac{1}{r}U+\frac{v}{2}\left(\frac{\mathrm{d}W}{\mathrm{d}r}\right)^2\right]\frac{1}{r}\frac{\mathrm{d}W}{\mathrm{d}r}\\ &\qquad+B_{11}\left(\frac{\mathrm{d}^3U}{\mathrm{d}r^3}+\frac{2}{r}\frac{\mathrm{d}^2U}{\mathrm{d}r^2}-\frac{1}{r^2}\frac{\mathrm{d}U}{\mathrm{d}r}+\frac{1}{r^3}U\right)+B_{11}\left[\frac{\mathrm{d}^3W}{\mathrm{d}r^3}+\frac{2-3v}{r}\frac{\mathrm{d}^2W}{\mathrm{d}r^2}-\frac{1}{r^2}\frac{\mathrm{d}W}{\mathrm{d}r}\right]\frac{\mathrm{d}W}{\mathrm{d}r}\\ &\qquad-N_r^{\mathrm{T}}\left(\frac{1}{r}\frac{\mathrm{d}W}{\mathrm{d}r}+\frac{\mathrm{d}^2W}{\mathrm{d}r^2}\right)+q. \end{aligned} \tag{17}$$

The continuity conditions at the center of plate results in W being finite, and

$$U=\frac{\mathrm{d}W}{\mathrm{d}r}=0,\quad \lim_{r\to 0}\left(\frac{\mathrm{d}^3W}{\mathrm{d}r^3}+\frac{1}{r}\frac{\mathrm{d}^2W}{\mathrm{d}r^2}\right)=0 \qquad \text{at } r=0.$$

In what follows, two types of boundary conditions are examined.

Case 1. The plate edge is clamped and immovable in r direction. Such that the boundary conditions can be expressed as

$$U=W=\frac{\mathrm{d}W}{\mathrm{d}r}=0 \quad \text{at } r=b. \tag{18}$$

Case 2. The plate edge is simply supported and immovable in r direction. Such that the boundary conditions can be expressed as

$$U=W=0,\quad B_{11}\left[\frac{\mathrm{d}U}{\mathrm{d}r}+\frac{v}{r}U+\frac{1}{2}\left(\frac{\mathrm{d}W}{\mathrm{d}r}\right)^2\right]-D_{11}\left(\frac{\mathrm{d}^2W}{\mathrm{d}r^2}+\frac{v}{r}\frac{\mathrm{d}W}{\mathrm{d}r}\right)-M_r^{\mathrm{T}}=0 \qquad \text{at } r=b. \tag{19}$$

Now, a nonlinear bending problem is formulated. If $q=0$, the problem reduces to a nonlinear buckling problem. It is difficult to solve such a nonlinear problem due to the inhomogeneity of material. For convenience, the following dimensionless parameters are introduced,

$$\begin{aligned} &x=\frac{r}{b},\quad w=\frac{W}{h},\quad u=\frac{Ub}{h^2},\quad F_1=\frac{B_{11}}{D_{11}}h,\quad F_2=\frac{A_{11}}{D_{11}}h^2,\quad F_3=\frac{B_{11}}{hA_{11}},\quad \overline{N}=\frac{N_r^{\mathrm{T}}b^2}{D_{11}},\quad \overline{M}=\frac{M_r^{\mathrm{T}}b^2}{D_{11}h},\\ &\lambda=12\frac{b^2}{h^2}(1+v)\alpha_{\mathrm{c}}T_2,\quad \overline{Q}=\frac{qb^4}{D_{11}h},\quad E_r=\frac{E_{\mathrm{m}}}{E_{\mathrm{c}}}. \end{aligned}$$

Such that the dimensionless governing equations and boundary conditions of the plate can be expressed as

$$\frac{\mathrm{d}^2u}{\mathrm{d}x^2}+\frac{1}{x}\frac{\mathrm{d}u}{\mathrm{d}x}-\frac{u}{x^2}+\frac{\mathrm{d}^2w}{\mathrm{d}x^2}\frac{\mathrm{d}w}{\mathrm{d}x}+\frac{1-v}{2x}\left(\frac{\mathrm{d}w}{\mathrm{d}x}\right)^2=F_3\left(\frac{\mathrm{d}^3w}{\mathrm{d}x^3}+\frac{1}{x}\frac{\mathrm{d}^2w}{\mathrm{d}x^2}-\frac{1}{x^2}\frac{\mathrm{d}w}{\mathrm{d}x}\right), \tag{20}$$

$$(1-F_1F_3)\left(\frac{\mathrm{d}^4w}{\mathrm{d}x^4}+\frac{2}{x}\frac{\mathrm{d}^3w}{\mathrm{d}x^3}-\frac{1}{x^2}\frac{\mathrm{d}^2w}{\mathrm{d}x^2}+\frac{1}{x^3}\frac{\mathrm{d}w}{\mathrm{d}x}\right)$$
$$=F_2\left[\frac{\mathrm{d}u}{\mathrm{d}x}+\frac{v}{x}u+\frac{1}{2}\left(\frac{\mathrm{d}w}{\mathrm{d}x}\right)^2\right]\frac{\mathrm{d}^2w}{\mathrm{d}x^2}+F_2\left[v\frac{\mathrm{d}u}{\mathrm{d}x}+\frac{1}{x}u+\frac{v}{2}\left(\frac{\mathrm{d}w}{\mathrm{d}x}\right)^2\right]\frac{1}{x}\frac{\mathrm{d}w}{\mathrm{d}x}$$
$$+F_1\left[\frac{2v}{x}\frac{\mathrm{d}^2w}{\mathrm{d}x^2}\frac{\mathrm{d}w}{\mathrm{d}x}+\frac{1}{x^2}\left(\frac{\mathrm{d}w}{\mathrm{d}x}\right)^2+\left(\frac{\mathrm{d}^2w}{\mathrm{d}x^2}\right)^2\right]-\overline{N}\left(\frac{1}{x}\frac{\mathrm{d}w}{\mathrm{d}x}+\frac{\mathrm{d}^2w}{\mathrm{d}x^2}\right)+\overline{Q}, \tag{21}$$

$$u=\frac{\mathrm{d}w}{\mathrm{d}x}=0,\quad \lim_{x\to 0}\left(\frac{\mathrm{d}^3w}{\mathrm{d}x^3}+\frac{1}{x}\frac{\mathrm{d}^2w}{\mathrm{d}x^2}\right)=0,\qquad w(0)=\xi \text{ at } x=0, \tag{22}$$

$$u=w=\frac{\mathrm{d}w}{\mathrm{d}x}=0 \quad \text{at } x=1, \tag{23}$$

or

$$u=w=0,\quad F_1\left[\frac{\mathrm{d}u}{\mathrm{d}x}+\frac{1}{2}\left(\frac{\mathrm{d}w}{\mathrm{d}x}\right)^2\right]-\left(\frac{\mathrm{d}^2w}{\mathrm{d}x^2}+\frac{v}{x}\frac{\mathrm{d}w}{\mathrm{d}x}\right)-\overline{M}=0 \qquad \text{at } x=1, \tag{24}$$

where ξ is a dimensionless deflection parameter.

3. Shooting method

In what follows, a shooting method (Li et al., 1996) is employed to numerically solve the problems. Here, the governing equations (20) and (21) and boundary conditions (22)–(24) can be rewritten in the following form

$$\frac{\mathrm{d}Y}{\mathrm{d}x}=H(x,Y), \tag{25}$$

$$B_0Y(0)=b_0, \tag{26a}$$

$$B_1Y(1)=b_1, \tag{26b}$$

where

$$Y=\{y_1\quad y_2\quad y_3\quad y_4\quad y_5\quad y_6\quad y_7\}^{\mathrm{T}}=\left\{w\quad \frac{\mathrm{d}w}{\mathrm{d}x}\quad \frac{\mathrm{d}^2w}{\mathrm{d}x^2}\quad \frac{\mathrm{d}^3w}{\mathrm{d}x^3}\quad u\quad \frac{\mathrm{d}u}{\mathrm{d}x}\quad \delta\right\}^{\mathrm{T}}, \tag{27}$$

$$H=\{y_2\quad y_3\quad y_4\quad \varphi\quad y_6\quad \psi\quad 0\}^{\mathrm{T}}. \tag{28}$$

For bending problem, $\delta=\overline{Q}$. For buckling and post-buckling problems, $\delta=\lambda$. Expressions of φ, ψ, B_0, B_1, b_0 and b_1 are as follows

$$\varphi = -\left(\frac{2}{x}\frac{\mathrm{d}^3 w}{\mathrm{d}x^3} - \frac{1}{x^2}\frac{\mathrm{d}^2 w}{\mathrm{d}x^2} + \frac{1}{x^3}\frac{\mathrm{d}w}{\mathrm{d}x}\right) + \left\{F_2\left[\frac{\mathrm{d}u}{\mathrm{d}x} + \frac{v}{x}u + \frac{1}{2}\left(\frac{\mathrm{d}w}{\mathrm{d}x}\right)^2\right]\frac{\mathrm{d}^2 w}{\mathrm{d}x^2}\right.$$
$$+ F_2\left[v\frac{\mathrm{d}u}{\mathrm{d}x} + \frac{1}{x}u + \frac{v}{2}\left(\frac{\mathrm{d}w}{\mathrm{d}x}\right)^2\right]\frac{1}{x}\frac{\mathrm{d}w}{\mathrm{d}x} + F_1\left[\frac{2v}{x}\frac{\mathrm{d}^2 w}{\mathrm{d}x^2}\frac{\mathrm{d}w}{\mathrm{d}x} + \frac{1}{x^2}\left(\frac{\mathrm{d}w}{\mathrm{d}x}\right)^2 + \left(\frac{\mathrm{d}^2 w}{\mathrm{d}x^2}\right)^2\right]$$
$$\left. - \overline{N}\left(\frac{1}{x}\frac{\mathrm{d}w}{\mathrm{d}x} + \frac{\mathrm{d}^2 w}{\mathrm{d}x^2}\right) + \overline{Q}\right\} \Big/ (1 - F_1 F_3), \tag{29}$$

$$\psi = -\left[\frac{1}{x}\frac{\mathrm{d}u}{\mathrm{d}x} - \frac{u}{x^2} + \frac{\mathrm{d}^2 w}{\mathrm{d}x^2}\frac{\mathrm{d}w}{\mathrm{d}x} + \frac{1-v}{2x}\left(\frac{\mathrm{d}w}{\mathrm{d}x}\right)^2\right] + F_3\left(\frac{\mathrm{d}^3 w}{\mathrm{d}x^3} + \frac{1}{x}\frac{\mathrm{d}^2 w}{\mathrm{d}x^2} - \frac{1}{x^2}\frac{\mathrm{d}w}{\mathrm{d}x}\right), \tag{30}$$

$$B_0 = \begin{bmatrix} 1 & 0 & 0 & 0 & 0 & 0 & 0 \\ 0 & 1 & 0 & 0 & 0 & 0 & 0 \\ 0 & 0 & 1/\Delta x & 1 & 0 & 0 & 0 \\ 0 & 0 & 0 & 0 & 1 & 0 & 0 \end{bmatrix}, \quad b_0 = \begin{Bmatrix} \xi \\ 0 \\ 0 \\ 0 \end{Bmatrix}. \tag{31}$$

For the clamped boundary, i.e. Case 1,

$$B_1 = \begin{bmatrix} 1 & 0 & 0 & 0 & 0 & 0 & 0 \\ 0 & 1 & 0 & 0 & 0 & 0 & 0 \\ 0 & 0 & 0 & 0 & 1 & 0 & 0 \end{bmatrix}, \quad b_1 = \begin{Bmatrix} 0 \\ 0 \\ 0 \end{Bmatrix}. \tag{32a}$$

For the simply supported boundary, i.e. Case 2,

$$B_1 = \begin{bmatrix} 1 & 0 & 0 & 0 & 0 & 0 & 0 \\ 0 & ((F_1 y_2)/2) - (v/\Delta x) & -1 & 0 & 0 & F_1 & 0 \\ 0 & 0 & 0 & 0 & 1 & 0 & 0 \end{bmatrix}, \quad b_1 = \begin{Bmatrix} 0 \\ \overline{M} \\ 0 \end{Bmatrix}. \tag{32b}$$

The small quantity Δx ($\Delta x > 0$) in Eqs. (31) and (32b) is introduced in computation to avoid the singularities of resultants of transverse shear force Q_r and moment M_r at $x = 0$.

Consider an initial value problem related to the boundary value problem Eqs. (25) and (26)

$$\frac{\mathrm{d}Z}{\mathrm{d}x} = H(x, Z), \tag{33a}$$

$$Z(\Delta x) = I(\xi, D), \tag{33b}$$

where

$$Z = \{\, z_1 \quad z_2 \quad z_3 \quad z_4 \quad z_5 \quad z_6 \quad z_7 \,\}^{\mathrm{T}},$$

$$I = \{\, \xi \quad 0 \quad d_1 \quad -d_1/\Delta x \quad 0 \quad d_2 \quad d_3 \,\}^{\mathrm{T}},$$

and the initial parameter vector,

$$D = \{\, d_1 \quad d_2 \quad d_3 \,\}^{\mathrm{T}}.$$

For a given value of parameter ξ, if there exists an initial parameter vector D such that Eqs. (33) satisfy Lipschitz condition, and the unique solution for the initial value problem must exist, namely,

$$Z(x; \delta, D) = I(D) + \int_{\Delta x}^{x} H(\xi, Z; \delta)\,\mathrm{d}\xi. \tag{34}$$

On the other hand, for the same value of ξ, if there exists $D^* = \{ d_1^* \quad d_2^* \quad d_3^* \}^{\mathrm{T}}$ such that $Z(x, \delta, D^*)$ satisfy

$$B_1 Z(x; \delta, D^*) = b_1, \tag{35}$$

one then obtains the following solution for the boundary value problem Eqs. (25) and (26)

$$Y(x; \delta) = Z(x; \delta, D^*). \tag{36}$$

This approach is called a shooting method.

4. Numerical results and discussions

In what follows, the well-known Runge–Kutta method in conjunction with a Newton iterative formulation are employed to numerically solve Eqs. (33) and (35). If one obtains the solution of Eqs. (25) and (26) for a sufficiently small value of parameter ξ, then the solutions of Eqs. (20)–(24) can be obtained for large scale of ξ by using the so-called analytical continuation method in which the parameter ξ increases step by step,

$$\delta = d_3^* = \delta(\xi), \quad \xi > 0. \tag{37}$$

For bending problem, Eq. (37) is the solution of deflection–load curves, $\overline{Q} = \overline{Q}(\xi)$. For post-buckling problem, Eq. (37) is the solution of post-buckling paths, $\lambda = \lambda(\xi)$.

Numerical analysis for the small deflection bending problem of a functionally graded circular plate with clamped and simply supported boundary conditions is carried out to examine the validity of the present numerical method. All the material parameters are taken from Reddy et al. (1999). Comparisons of the numerical results obtained in the present paper to the analytical results obtained by Reddy et al. (1999) are shown in Table 1 for the dimensionless deflection $w^* = 64WD_c/qb^4$ at the center of plate. Excellent agreements can be seen from Table 1, and the validity of the present numerical method is verified.

Table 1
Comparisons of the results obtained in the present paper to the results obtained by Reddy et al. (1999) for the maximum dimensionless deflection w^* of FGM circular plate with different material constant n and different boundary conditions under uniformly distributed transverse mechanical loading ($v = 0.288$, $E_r = E_m/E_c = 0.396$)

Material constant n	Reddy et al. (1999)		Present paper	
	Clamped plate	Simply supported plate	Clamped plate	Simply supported plate
0	2.525	10.368	2.525	10.368
2	1.388	5.483	1.389	5.485
4	1.269	5.102	1.269	5.103
6	1.208	4.897	1.208	4.899
8	1.169	4.761	1.169	4.762
10	1.143	4.665	1.143	4.665
15	1.103	4.514	1.103	4.514
20	1.080	4.426	1.080	4.427
25	1.066	4.370	1.066	4.370
30	1.056	4.330	1.056	4.330
35	1.048	4.301	1.048	4.301
40	1.043	4.278	1.043	4.278
50	1.034	4.246	1.034	4.246
100	1.018	4.178	1.018	4.178

4.1. Temperature field

In what follows, a metal, aluminum and ceramics, zirconia system of FGM is considered. The material parameters, Young's modulus E, Poisson's ratio v, thermal conductivity and thermal expansion coefficients K and α are taken from Praveen and Reddy (1998) and Reddy (2000) which are summarized in Table 2. Dimensionless parameters $W(0)/h$—center deflection and $Q = qb^4/D_c h$—load parameter are used in analysis, and $T_1/T_2 = 15$.

Fig. 1 shows the variations of volume fraction of metallic phase through the thickness of plate for various values of n calculated from Eq. (2). If $n = 0$ the plate reduces to a pure metallic plate. Temperature distributions through the thickness of the functionally graded plate for various values of n calculated from Eq. (11) are shown in Fig. 2. It is seen that temperature in the functionally graded plate is always lower than that in a pure metallic plate (i.e. $n = 0$). Effect of n on the mid-plane temperature in the plate is shown in Fig. 3. It is clear that the mid-plane temperature reaches a minimum value at $n = 3$. As the material constant n increases from 0 to 3, the mid-plane temperature decreases rapidly, after that it increases rapidly as n increases from 3 to 20, and then it increases slowly as $n > 20$.

4.2. Nonlinear bending of the FGM plate

In this section, nonlinear bending of a functionally graded circular plate is numerically analyzed under the thermal, uniformly distributed transverse mechanical and combined thermal–mechanical loadings.

Table 2
Material parameters of metal, aluminum and ceramics, zirconia in the FGM system (Praveen and Reddy, 1998; Reddy, 2000)

Materials	Young's modulus E (GPa)	Poisson's ratio v	Thermal conductivity coefficient K (W/mk)	Thermal expansion coefficient α (1/°C)
Aluminum	70	0.3	204	23×10^{-6}
Zirconia	151	0.3	2.09	10×10^{-6}

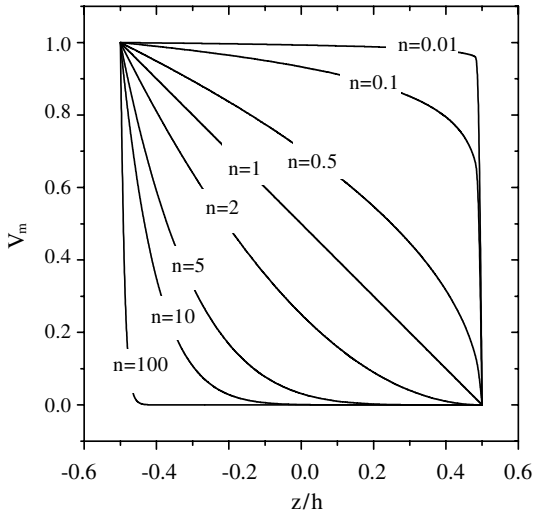

Fig. 1. Variations of the volume fraction of metallic phase through the dimensionless thickness of the functionally grated plate for different values of n.

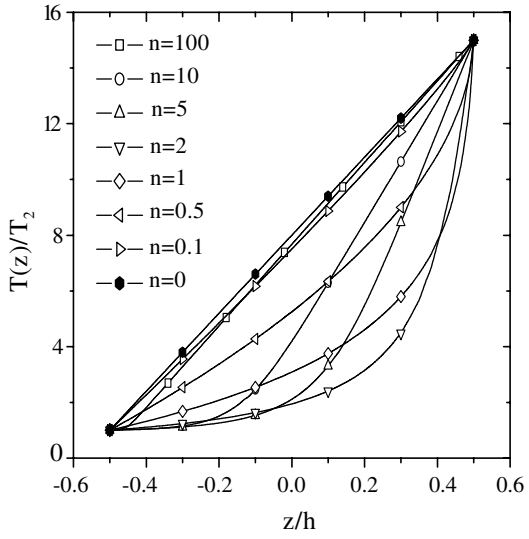

Fig. 2. Temperature distributions through the thickness of FGM plate for different values of material constant n.

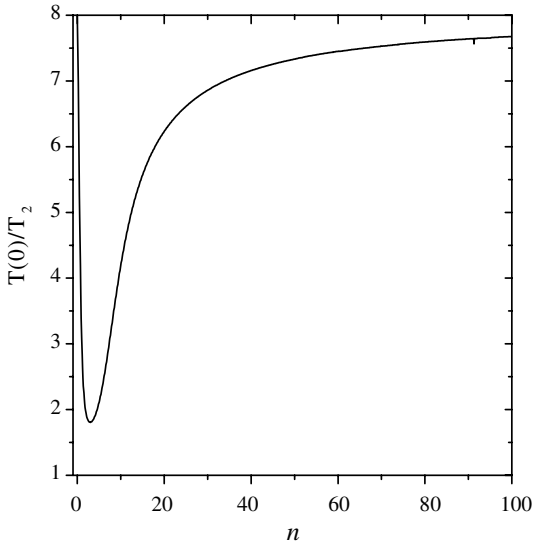

Fig. 3. Effect of material constant n on the temperature at the mid-plane of FGM plate ($z = 0$).

Figs. 4 and 5 show respectively the curves of dimensionless deflection at the center of the clamped and simply supported FGM plates vs. the uniformly distributed transverse mechanical load parameter Q for different values of material constant n. It is clear that the center deflection in the FGM plate is lower than that of pure metallic plate (i.e. $n = 0$), and this deflection decreases significantly with increasing the value of n for the same value of transverse mechanical load. This is because pure metallic plate has lower stiffness than the functionally graded plate. The greater the value of mechanical load, the more significant the effect of the material constant n on the center deflection in FGM plate. In the case of the combined thermal–

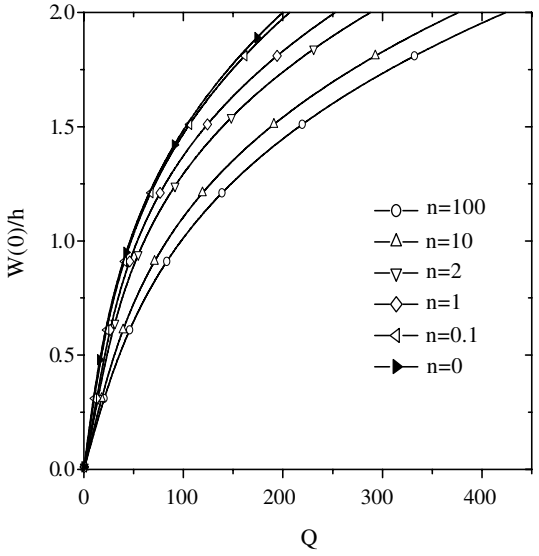

Fig. 4. Deflection vs. transverse mechanical load for the clamped FGM plate with different values of n.

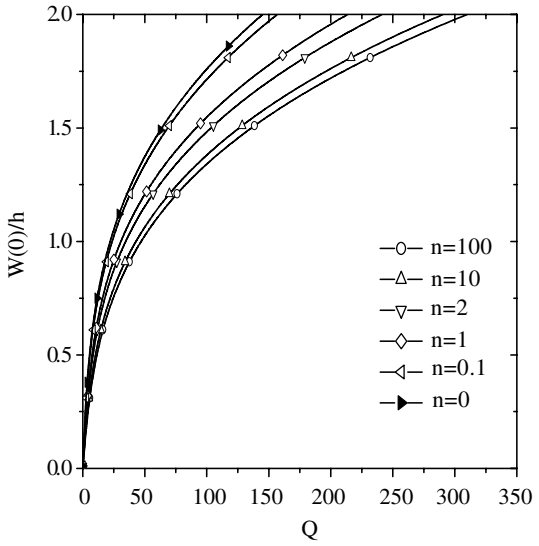

Fig. 5. Deflection vs. transverse mechanical load for the simply supported FGM plate with different values of n.

mechanical loading, these phenomenon are still true, see the dashed lines shown in Figs. 6 and 7, respectively. It is also seen from Figs. 6 and 7 that effect of thermal load on the deflection of pure metallic plate ($n = 0$) is greater than that of FGM plate.

Effect of material constant n on the center deflection of FGM plates with and without thermal load is shown in Figs. 8 and 9 for clamped and simply supported boundary conditions, respectively. The dashed lines denote the case of combined thermal–mechanical loading. One can seen from Figs. 8 and 9 that the center deflection in FGM plate decreases rapidly as the material constant n increases from 0 to 5 for the

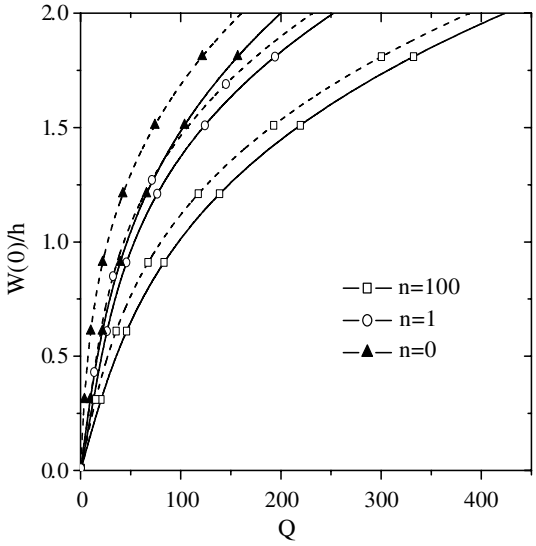

Fig. 6. Comparisons of the curves of transverse mechanical load vs. center deflection of clamped FGM plates with and without thermal loading. The dashed lines denote the case of thermal load parameter $\lambda = 0.5$.

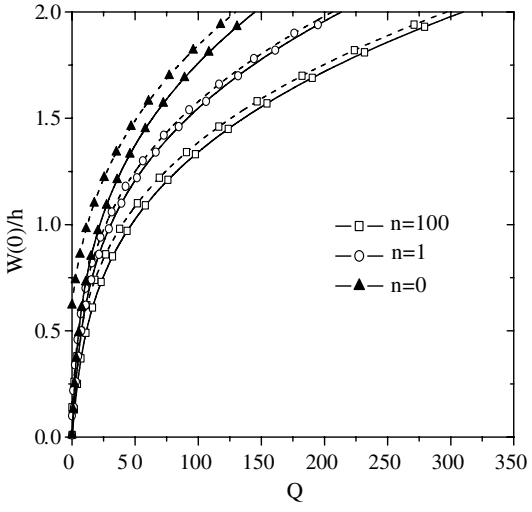

Fig. 7. Comparisons of the curves of transverse mechanical load vs. center deflection of simply supported FGM plates with and without thermal loading. The dashed lines denote the case of thermal load parameter $\lambda = 0.2$.

same values of mechanical load. As $n > 5$, effect of n becomes not so significant. In the case of combined thermal–mechanical loading, these phenomena are still true, for more details see the dashed lines shown in Figs. 8 and 9. It is valuable to note that combined thermal–mechanical loading results in a higher value of center deflection in the FGM plate for the same value of material constant n.

The temperature filed Eq. (11) applied individually to a simply supported FGM plate yields bending deflection in the plate gradually from the beginning of heating. However, one cannot see this phenomenon

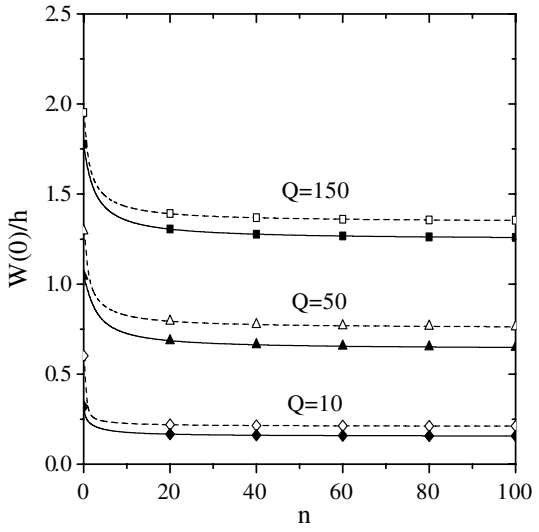

Fig. 8. Effects of material constant n and mechanical load parameter Q on the center deflection of the clamped FGM plate with and without thermal loading. The dashed lines denote the case of combining thermal–mechanical loading with the thermal load parameter $\lambda = 0.5$.

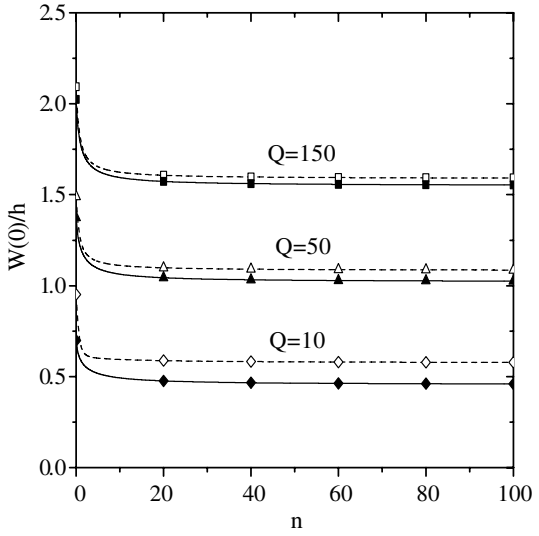

Fig. 9. Effects of material constant n and mechanical load parameter Q on the center deflection of the simply supported FGM plate with and without thermal loading. The dashed lines denote the case of combining thermal–mechanical loading with the thermal load parameter $\lambda = 0.2$.

in the case of the clamped FGM plate. In other words, the boundary condition has important effect on the behavior mode of a functionally graded plate. Figs. 10 and 11 show the thermal load–deflection curves of the simply supported FGM plate for different values of material constant n. It is seen that material constant

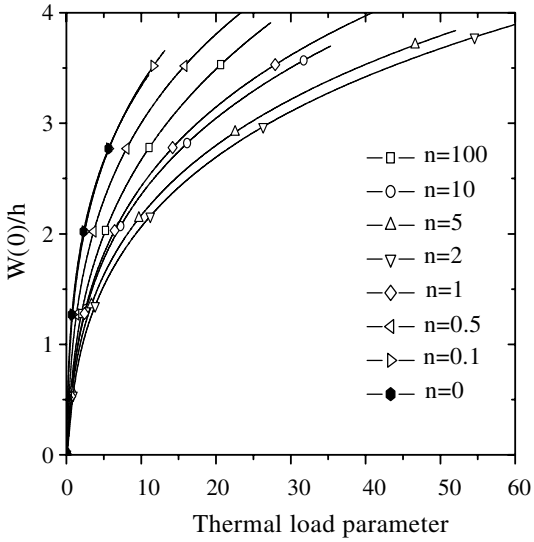

Fig. 10. Curves of thermal load vs. center deflection of the simply supported FGM plate for different values of material constant n.

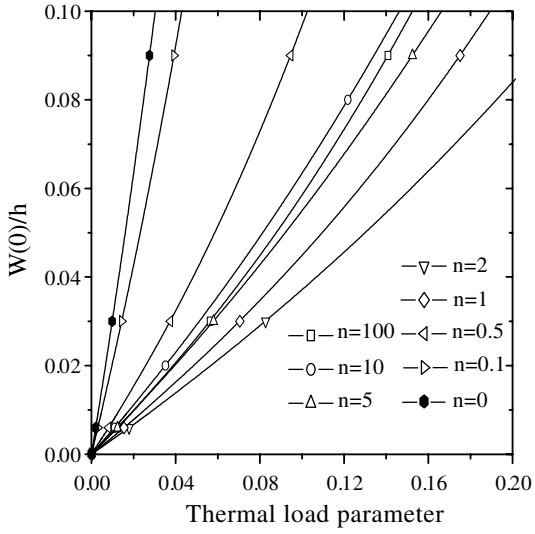

Fig. 11. A part of Fig. 10 for the small values of $W(0)/h$.

n has significant effect on the thermal bending behavior of the FGM plate, which is different from that of Fig. 5. One can see from Fig. 11 that deflection in the simply supported FGM plate increases almost linearly with increasing thermal load when values of thermal load parameter λ is small, saying, $\lambda < 0.2$.

Bending configurations of the clamped and simply supported FGM plates subjected to the combined thermal–mechanical loading (dashed lines) and individual mechanical loading (solid lines) are respectively shown in Figs. 12 and 13 for the mechanical load parameter $Q = 100$. Bending configurations of the simply

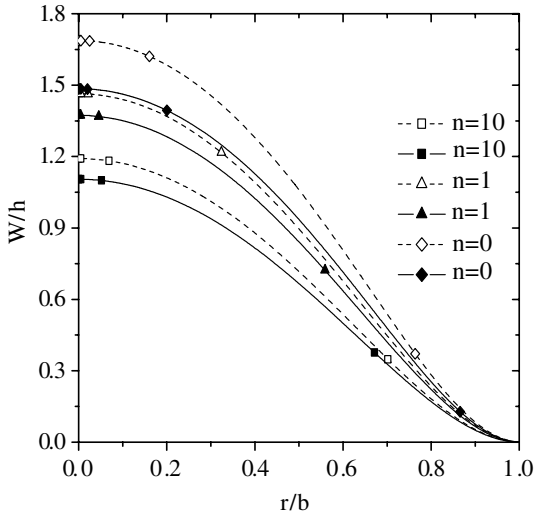

Fig. 12. Bending configurations of the clamped FGM plate subjected to the combining thermal–mechanical loading (dashed lines) and individual mechanical loading (solid lines) for different values of material constant n. The mechanical load parameter $Q = 100$.

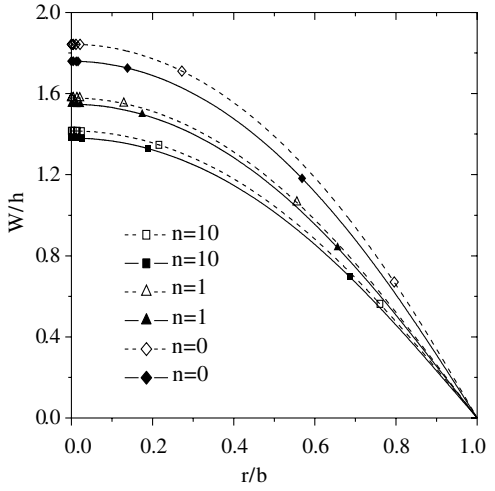

Fig. 13. Bending configurations of the simply supported FGM plate subjected to the combining thermal–mechanical loading (dashed lines) and individual mechanical loading (solid lines) for different values of material constant n. The mechanical load parameter $Q = 100$.

supported FGM plate subjected to individual thermal load $\lambda = 5$ are shown in Fig. 14. It is clear that deflection of the FGM plate is lower than that of pure metallic plate (i.e. $n = 0$). In the cases of individual mechanical loading and the combined thermal–mechanical loading, deflection of the plate decreases with the increase of material constant n. However, the deflection decreases as n increases from 0 to ≈ 3, and it increases as $n > 3$ in the case of individual thermal loading, which is related to the temperature distribution shown in Fig. 3.

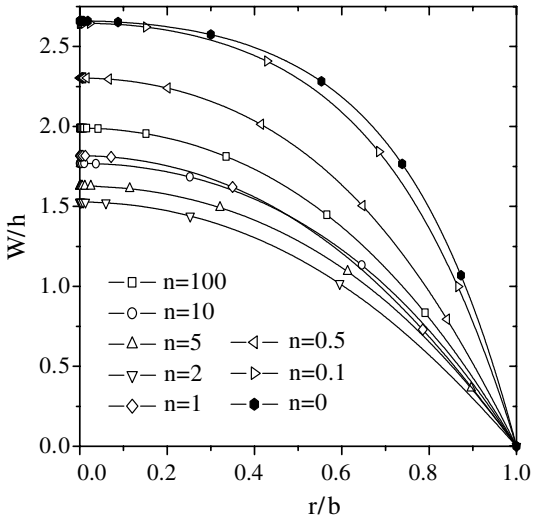

Fig. 14. Bending configurations of the simply supported FGM plate with individual thermal load parameter $\lambda = 5$ for different values of material constant n.

4.3. Thermal buckling and post-buckling of the FGM plate

Thermal buckling and post-buckling behavior of a functionally graded plate is studied in this section. Fig. 15 shows the effect of material constant n on the critical buckling temperature λ_{cr} of the clamped FGM plate. It is clear that the value of critical buckling temperature for the clamped FGM plate is greater than that of the pure metallic plate (i.e. $n = 0$). The critical buckling temperature increases rapidly as the material constant n increases from 0 to 2, and it decreases rapidly as n increases from 2 to 20. As $n > 20$, λ_{cr} decreases

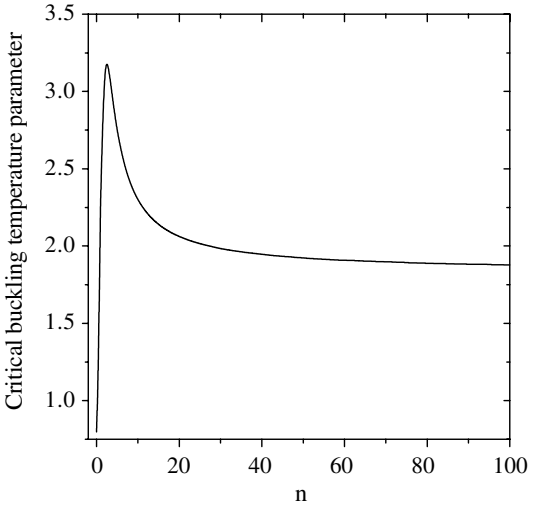

Fig. 15. Effect of the material constant n on the critical buckling temperature λ_{cr} of the clamped FGM plate.

very slowly. This means that the thermal stability of FGM plate is better than that of the pure metallic plate.

Thermal post-buckling paths for the clamped FGM plate are respectively shown in Figs. 16 and 17 for different values of material constant n. It is seen that the material constant n has significant effect on the thermal post-buckling behavior of FGM plate, especially in the case of large deflection. An interesting phenomenon in Fig. 17 is that for the clamped FGM plate, the post-buckling temperature does not increase monotonically with increasing the center deflection. Especially in the cases of $n = 0.5$, 1, 2 and 5, the post-buckling temperature decreases at first, and then increases with the increase of deflection. This means that

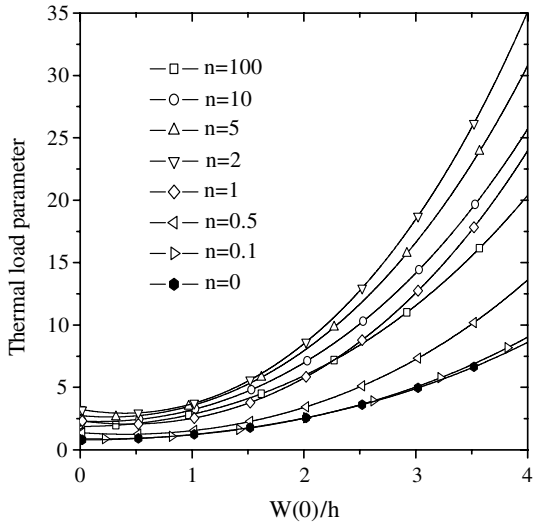

Fig. 16. Curves of post-buckling thermal load vs. center deflection of the clamped FGM plate for different values of material constant n.

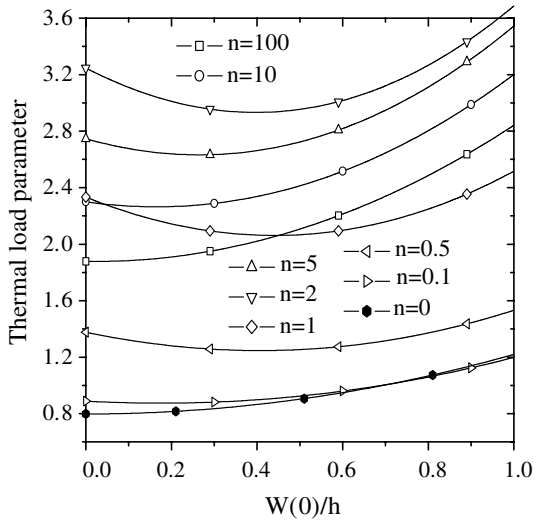

Fig. 17. A part of Fig. 16 for the small values of $W(0)/h$.

the thermal post-buckling behavior of a functionally graded plate is quite different from that of a homogenous plate, if the difference of volume fraction of two constituents is small.

Effect of material constant n on the thermal bending and thermal post-buckling deflection in the simply supported and clamped FGM plates are respectively shown in Fig. 18 in the case of thermal load parameter $\lambda = 5$. It is seen that the thermal post-buckling deflection and thermal bending deflection decreases rapidly as n increases from 0 to $\approx$2.5, after then it increases slowly with increasing n. Effect of material constant n on the thermal post-buckling configurations of the clamped FGM plate are shown in Fig. 19. It is clear that

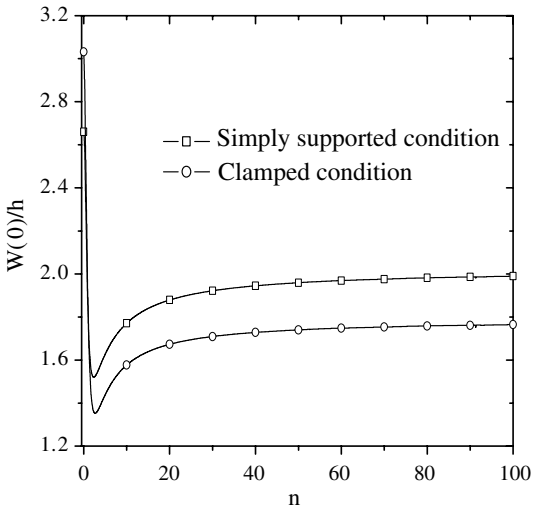

Fig. 18. Effect of material constant n on the thermal bending and thermal post-buckling deflection $W(0)/h$ in the simply supported and clamped FGM plates, respectively, with thermal load parameter $\lambda = 5$.

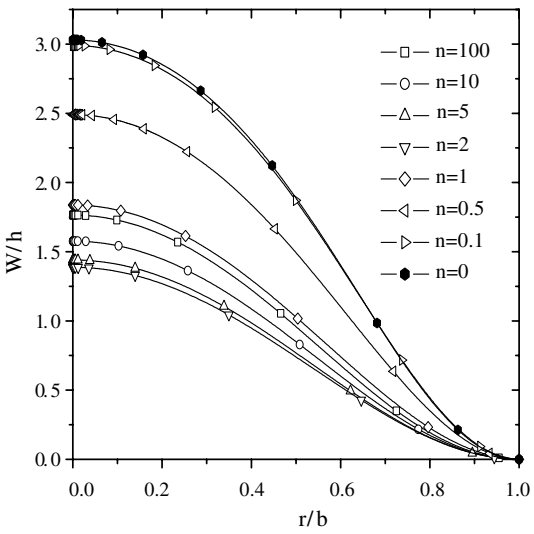

Fig. 19. Thermal post-buckling configurations of the clamped FGM plate with thermal load parameter $\lambda = 5$ for different values of material constant n.

the thermal post-buckling deflection of the clamped FGM plate is lower than that of a pure metallic plate (i.e. $n = 0$), and it decreases with the increase of material constant n. In other words, material constant n has important effect on the thermal post-buckling configurations of FGM plate.

5. Conclusions

Axisymmetric nonlinear bending and thermal post-buckling of a functionally graded circular plate are investigated under uniformly distributed transverse mechanical, thermal and combined mechanical–thermal loadings, respectively. Based on the classical nonlinear von Karman plate theory, governing equations for the problem are derived, and then a shooting method is employed to numerically solve the equations. Effects of material constant n and boundary conditions on the temperature distribution, nonlinear bending, critical buckling temperature and thermal post-buckling behavior of the FGM plate are discussed in details. The following conclusions are addressed:

Temperature distribution through the thickness of the functionally graded plate is always lower than that in a pure metallic plate. The material constant n has significant effect on the mid-plane temperature in the FGM plate.

Deflection in the center of FGM plate is lower than that of a pure metallic plate, and this deflection decreases significantly with increasing the value of n. The greater the value of load, the more significant the effect of material constant n on the center deflection in FGM plate. In the case of combined thermal–mechanical loading, these phenomena are still true. It is valuable to note that the combined thermal–mechanical loading results in a great value of center deflection in the FGM plate for the same value of material constant n.

Material constant n has important effect on the critical buckling temperature of the clamped FGM plate. This critical temperature is higher than that of a pure metallic plate. In the other words, the thermal stability of FGM plate is better than that of a pure metallic plate. The material constant n has significant effect on the thermal post-buckling behavior of FGM plate, especially for the problem of large deflection. Boundary condition has important effect on the behavior modes of a functionally graded plate subjected to an individual temperature field Eq. (11). The post-buckling temperature does not increase monotonically with increasing the center deflection for the clamped FGM plate.

Acknowledgements

This work was supported by the National Natural Science Foundation of China (10125212) and the Fund from The Ministry of Education of China.

References

Almajid, A., Taya, M., Hudnut, S., 2001. Analysis of out-of-plane displacement and stress field in a piezocomposite plate with functionally graded microstructure. International Journal of Solids and Structures 38, 3377–3391.

Cheng, Z.Q., 2001. Nonlinear bending of inhomogeneous plates. Engineering Structures 23, 1359–1363.

Cheng, Z.Q., Batra, R.C., 2000. Three-dimensional thermo-elastic deformations of a functionally graded elliptic plates. Composites, Part B 31, 97–106.

Feldman, E., Aboudi, J., 1997. Buckling analysis of functionally graded plates subjected to uniaxial loading. Composite Structure 38, 29–36.

Gong, S.W., Lam, K.Y., Reddy, J.N., 1999. The elastic response of functionally graded cylindrical shells to low-velocity impact. International Journal of Impact Engineering 22, 397–417.

Javaheri, R., Eslami, M.R., 2002a. Thermal buckling of functionally graded plates. AIAA Journal 40, 162–169.
Javaheri, R., Eslami, M.R., 2002b. Thermal buckling of functionally graded plates based on higher order theory. Journal of Thermal Stresses 25, 603–625.
Leissa, A.W., 1992. Review of recent developments in laminated composite plate buckling analysis. Composite Material Technology 45, 1–7.
Li, S.R., Zhao, Y.G., Ma, L.S., 1996. Shooting method for solving the axisymmetric von Karman equations in terms of displacements. Mechanics and Practice 18 (4), 24–26 (in Chinese).
Loy, C.T., Lam, K.Y., Reddy, J.N., 1999. Vibration of functionally graded cylindrical shells. International Journal of Solids and Structures 41, 309–324.
Ma, L.S., Wang, T.J., in press. Axisymmetric post-buckling of a functionally graded circular plate subjected to uniformly distributed radial compression. Materials Science Forum.
Meyers, C.A., Hyer, M.W., 1991. Thermal buckling and post-buckling of symmetrically laminated composite plates. Journal of Thermal Stresses 14, 519–540.
Mian, M.A., Spencer, J.M., 1998. Exact solution for functionally graded and laminated elastic materials. Journal of the Mechanics and Physics of Solids 46, 2283–2295.
Ng, T.Y., Lam, K.Y., Liew, K.M., 2000. Effects of FGM material on the parametric resonance of plate structures. Computer Methods in Applied Mechanics and Engineering 190, 953–962.
Ng, T.Y., Lam, K.Y., Liew, K.M., Reddy, J.N., 2001. Dynamic stability analysis of functionally graded cylindrical shells under periodic axial loading. International Journal of Solids and Structures 38, 1295–1309.
Pradhan, S.C., Loy, C.T., Reddy, J.N., 2000. Vibration characteristics of functionally graded cylindrical shells under various boundary conditions. Applied Acoustics 61, 119–129.
Praveen, G.N., Reddy, J.N., 1998. Nonlinear transient thermoelastic analysis of functionally graded ceramic–metal plates. International Journal of Solids and Structures 35, 4457–4476.
Reddy, J.N., 2000. Analysis of functionally graded plates. International Journal for Numerical Methods in Engineering 47, 663–684.
Reddy, J.N., Cheng, Z.Q., 2001. Three-dimensional thermo-mechanical deformations of functionally graded rectangular plates. European Journal of Mechanics A/Solids 20, 841–855.
Reddy, J.N., Chin, C.D., 1998. Thermomechanical analysis of functionally graded cylinders and plates. Journal of Thermal Stresses 21, 593–626.
Reddy, J.N., Wang, C.M., Kitipornchai, S., 1999. Axisymmetric bending of functionally graded circular and annular plates. European Journal of Mechanics A/Solids 18, 185–199.
Tauchert, T.R., 1991. Thermally induced flexure, buckling and vibration of plates. Applied Mechanics Review 44, 347–360.
Tauchert, T.R., Huang, W.N., 1987. Thermal buckling of symmetric angle-ply laminated plates. Composite Structures 4, 424–435.
Woo, J., Meguid, S.A., 2001. Nonlinear analysis of functionally graded plates and shallow shells. International Journal of Solids and Structures 38, 7409–7421.
Yang, J., Shen, H.S., 2001. Dynamic response of initially stressed functionally graded rectangular thin plates. Composite Structures 54, 497–508.